Sodium Batteries | Hot Paper

DOI: 10.1002/ange.201400032

All Organic Sodium-Ion Batteries with $Na_4C_8H_2O_6$**

*Shiwen Wang, Lijiang Wang, Zhiqiang Zhu, Zhe Hu, Qing Zhao, and Jun Chen**

Abstract: *Developing organic compounds with multifunctional groups to be used as electrode materials for rechargeable sodium-ion batteries is very important. The organic tetrasodium salt of 2,5-dihydroxyterephthalic acid (Na_4DHTPA; $Na_4C_8H_2O_6$), which was prepared through a green one-pot method, was investigated at potential windows of 1.6–2.8 V as the positive electrode or 0.1–1.8 V as the negative electrode (vs. Na^+/Na), each delivering compatible and stable capacities of ca. 180 mAh g^{-1} with excellent cycling. A combination of electrochemical, spectroscopic and computational studies revealed that reversible uptake/removal of two Na^+ ions is associated with the enolate groups at 1.6–2.8 V ($Na_2C_8H_2O_6$/$Na_4C_8H_2O_6$) and the carboxylate groups at 0.1–1.8 V ($Na_4C_8H_2O_6$/$Na_6C_8H_2O_6$). The use of $Na_4C_8H_2O_6$ as the initial active materials for both electrodes provided the first example of all-organic rocking-chair SIBs with an average operation voltage of 1.8 V and a practical energy density of about 65 Wh kg^{-1}.*

Room-temperature rechargeable sodium-ion batteries (SIBs) have recently become a research focus because sodium has a high natural abundance, low cost, and is more environmentally benign than lithium.[1–3] However, similar to Li-ion batteries (LIBs), an overwhelming majority of host materials in SIBs are based on depletable transition-metal inorganic compounds,[4–9] which are generally prepared from limited mineral resources through energy intensive processing. The development of new types of green and sustainable Na-storage materials is therefore necessary for safer and less-expensive rechargeable SIBs.

One of the innovative strategies is shifting from traditional inorganic compounds to new organic alternatives. Organic concept provides potential advantages such as structural diversity and flexibility, molecular level controllability, eco-efficient processability and resource renewability.[10–13] Indeed, a series of organic compounds have been studied as the electrode materials of energy-storage devices such as LIBs and supercapacitors.[14–24] Recently, some of them have been demonstrated to have high specific capacity, cycling stability, and high rate capability, making them promising applications in SIBs.[25–31] However, there are only a few reports on sodium-ion full cells based on organic electrode materials. Abouimrane et al.[32] first incorporated a disodium terephthalate-based organic anode material into sodium-ion full cells, but a conventional transition-metal cathode material ($Na_{0.75}Mn_{0.7}Ni_{0.23}O_2$) was still needed. The first and only all organic sodium-ion cell based on a polymeric cathode and anode was constructed by Yang and co-workers,[33] showing a specific capacity of ca. 55 Wh kg^{-1} with an average voltage of 1.8 V. In this system, a p-doped polymer was used as a cathode material, which experiences the p-doping/de-doping mechanism of large electrolyte anions, causing the consumption of a large amount of electrolyte, and thus tremendously reducing the practical specific energy of the batteries. From this point of view, finding suitable Na-reservoir positive and negative organic electrode materials and developing all-organic rocking-chair SIBs analogous to the well-known lithium-ion system[10,34,35] is of great significance and challenge.

Herein, we report the electrochemical performance of a novel organic tetrasodium salt Na_4DHTPA with enolate and carboxylate groups as the electrode materials of room-temperature rechargeable SIBs. It is demonstrated that two reversible two-Na^+-ion electrochemical reactions occur with redox couples of $Na_2C_8H_2O_6$/$Na_4C_8H_2O_6$ as the positive electrode at 2.3 V and $Na_4C_8H_2O_6$/$Na_6C_8H_2O_6$ as the negative electrode at 0.3 V, respectively. Both the positive and negative electrodes can deliver reversible capacities of higher than 180 mAh g^{-1} with excellent cycling. Furthermore, starting from the Na-reservoir Na_4DHTPA as both the positive and negative active materials, we have successfully fabricated an all organic rocking-chair Na-ion battery with an average output voltage of 1.8 V. This result should shed light on the design and application of organic materials for room-temperature rechargeable SIBs.

The molecular structure of Na_4DHTPA and the corresponding redox reactions are shown in Scheme 1. The organic small molecule couples both phenolic enolate groups and carboxylate groups at the two para positions of one benzene ring, offering a theoretical specific capacity of 187 mAh g^{-1}, whether $Na_4C_8H_2O_6$ is used as the positive electrode or as the negative electrode. The electron delocalization effect of

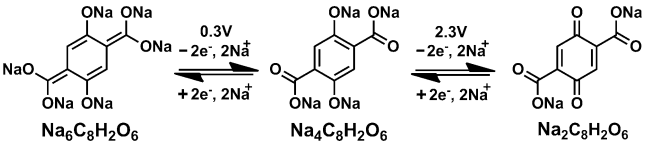

Scheme 1. Electrochemical redox reaction mechanism of Na^+ ions with $Na_4C_8H_2O_6$/$Na_6C_8H_2O_6$ and $Na_2C_8H_2O_6$/$Na_4C_8H_2O_6$ at potentials of 0.3 V and 2.3 V, respectively.

[*] Dr. S. W. Wang, Dr. L. J. Wang, Dr. Z. Q. Zhu, Z. Hu, Dr. Q. Zhao, Prof. Dr. J. Chen
Key Laboratory of Advanced Energy Materials Chemistry (Ministry of Education), College of Chemistry, Collaborative Innovation Center of Chemical Science and Engineering
Nankai University, Tianjin 300071 (China)
E-mail: chenabc@nankai.edu.cn

[**] This work was supported by Programs of National 973 (2011CB935900), NSFC (21231005 and 51231003) and MOE (B12015 and 113016A).

Supporting information for this article is available on the WWW under http://dx.doi.org/10.1002/anie.201400032.

carboxylate groups and the electron-donating ability of enolate sites contribute separately to a positive shift in de-sodiation potential and a negative shift in sodiation potential, which favorably enlarges the potential gap of both redox couples. Moreover, the conjugation effects of each functional group with a robust benzene core can effectively stabilize the as-produced redox species in electrochemical process. Most importantly, the formation of a tetrasodium salt not only overcomes the dissolution problem in aprotic electrolytes that often relates to small molecules, but also provides Na^+ ions of the enolate sites functioning as a Na-reservoir pool to avoid the use of sodium metal with potential safety risks.

The target Na_4DHTPA was synthesized for the first time by a green one-pot reaction of 2,5-dihydroxyterephthalic acid (DHTPA) with sodium hydroxide in aqueous solution (for experimental details, see Scheme S1 in the Supporting Information). The raw material, DHTPA, is a low-cost chemical commodity and can be mass produced by the carboxylation of hydroquinone. FTIR (Figure S1), NMR (Figure S2), and MS (Figure S3) spectra, and elemental analysis (Table S1) all clearly indicate the formation of the tetrasodium salt Na_4DHTPA from DHTPA. The resulting Na_4DHTPA is in the form of a yellow powder with low crystallinity (Figure S4) and rod-like morphology (Figure S5 a,b). The rods are micrometers in length and tens to hundreds of nanometers in width/diameter. The compositions of the as-prepared Na_4DHTPA rods were further confirmed by elemental mapping analysis and energy dispersive X-ray (EDX). Sodium, carbon, and oxygen are homogeneously distributed throughout (Figure S5 c–f). The Brunauer-Emmett-Teller (BET) specific surface area of the rods was measured to be 103.8 $m^2 g^{-1}$ (Figure S6). In addition, thermogravimetric analysis of Na_4DHTPA rods in Ar atmosphere (Figure S7) reveals that there is no weight loss from 33 to 250 °C and only $<5\%$ weight loss between 300 and 500 °C. This shows that Na_4DHTPA has respectable thermal stability, which is a key factor in the safety of rechargeable batteries.

To evaluate the practical feasibility of $Na_4C_8H_2O_6$ as a positive or a negative electrode material, CR2032 coin-type $Na_4C_8H_2O_6$/Na half cells were assembled and tested either at a high voltage range of 1.6–2.8 V or at a lower voltage region of 1.8–0.1 V at room temperature (298 K). The CR2032 half cells consist of a $Na_4C_8H_2O_6$ cathode and sodium-metal anode separated by a porous glass-fiber film. The electrolyte is $NaClO_4$ (1 M) in 1:1 (*v*/*v*) ethylene carbonate/dimethyl carbonate (EC/DMC; for electrochemical measurements, see the Supporting Information).

Figure 1 displays the electrochemical performance of $Na_4C_8H_2O_6$ at 1.6–2.8 V versus Na^+/Na. The cyclic voltammogram (CV) curves (Figure 1 a) show that in the first cycle, only one sharp oxidation peak at 2.57 V and a pair of reduction peaks at 2.36 and 2.1 V were observed with a nearly equivalent integral area of redox peaks. After the first cycle, a pair of sharp peaks at 2.56/2.36 V and two weak shoulder peaks at 2.35/2.1 V emerge; these peaks have similar intensities and areas, respectively, and remain almost unchanged in the subsequent cycles, which indicates a two-step 2 e^- redox reaction of the enolate groups in $Na_4C_8H_2O_6$. As demonstrated in Scheme 1, the redox reaction of $Na_4C_8H_2O_6$ at an

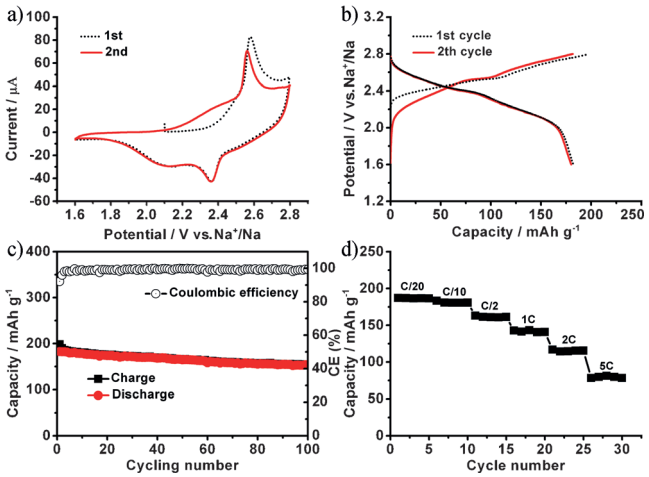

Figure 1. Electrochemical performance of $Na_4C_8H_2O_6$/Na half cells in the voltage range of 1.6–2.8 V vs. Na^+/Na: a) CV curves at a scan rate of 0.1 $mV s^{-1}$. b) The initial discharge/charge profiles at a rate of C/10 (19 $mA g^{-1}$). c) Cycling and coulombic efficiency at a rate of C/10. and d) Rate capability at various rates from C/20 to 5 C.

average potential of 2.3 V takes place between enolate and quinonoid carbonyl groups ($Na_2C_8H_2O_6$/$Na_4C_8H_2O_6$), accompanied by the extraction/insertion of Na^+ ions from/into $Na_4C_8H_2O_6$. The initial anodic peak can be regarded as an electrochemical activation process. This phenomenon was previously observed with the Li-storage positive electrode of $Li_4C_8H_2O_6$, namely the tetralithium salt of DHTPA.[36] Figure 1 b shows the typical galvanostatic charge/discharge profiles of the cells cycled between 1.6 and 2.8 V. Apart from the first charge occurring at a slightly higher potential, all curves show similar features and present two slope-shape plateaus and a low potential gap around 0.2 V. The first Coulombic efficiency of 92 % demonstrated that irreversible electrochemical reactions occurred in the initial de-sodiation process. The initial discharge capacity was 183 $mAh g^{-1}$ at C/10 (*n* C, or C/*n* when $n = 1/n$, corresponds to charging or discharging the full capacity in 1/*n* h; 1 C = 187 $mA g^{-1}$), and the capacity retention of more than 84 % was maintained after 100 cycles (Figure 1 c). The excellent capacity retention is attributed to the high structural stability and insolubility (or extremely low solubility) of $Na_4C_8H_2O_6$ in the electrolyte because of strong intermolecular interactions occurring in the crystalline solid. In addition to high capacity retention, the Coulombic efficiency is close to 100 % after a few cycles. Furthermore, the electrode exhibits a high rate capability up to 5 C (Figure 1 d).

Figure 2 a shows the CVs of $Na_4C_8H_2O_6$ between 1.8 V and 0.1 V vs. Na^+/Na. During the first cathodic scan, a weak hump occurs from 1.1 V to 0.40 V and disappears in the subsequent scans, implying an irreversible decomposition of the electrolyte for the formation of solid–electrolyte interface (SEI) films. A reduction peak at 0.12 V can be assigned to the insertion reaction of Na^+ ions into $Na_4C_8H_2O_6$ to form the compound $Na_6C_8H_2O_6$. During the anodic scan, one broad oxidation peak emerges at 0.40 V, corresponding to the extraction reaction of Na^+ ions from $Na_6C_8H_2O_6$ to form $Na_4C_8H_2O_6$. In the following scans, the CV curves show a pair

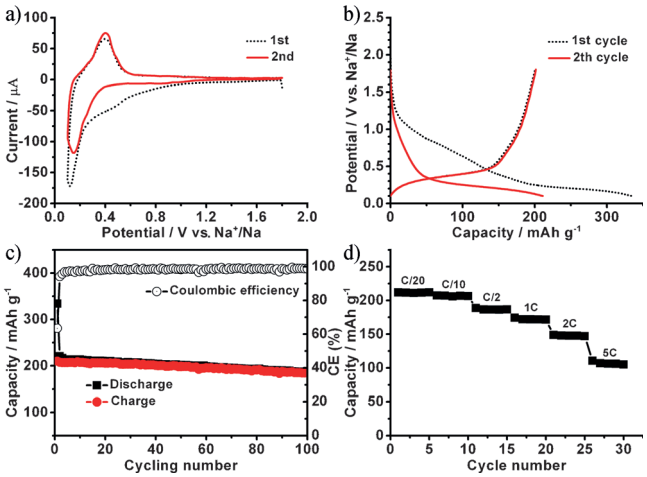

Figure 2. Electrochemical performance of $Na_4C_8H_2O_6$/Na half cells in the voltage range of 1.8–0.1 V vs. Na^+/Na: a) CV curves at a scan rate of 0.1 mV s^{-1}. b) The initial discharge/charge profiles at a rate of C/10 (19 mA g^{-1}). c) Cycling and Coulombic efficiency at a rate of C/10. d) Rate capability at various rates from C/20 to 5 C.

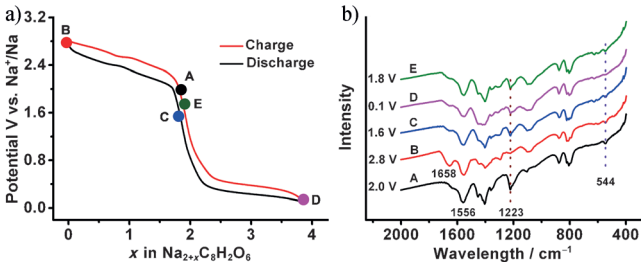

Figure 3. Structural evolution of $Na_4C_8H_2O_6$ in the full potential window of 0.1–2.8 V: a) A potential-composition profile at a C/10 rate. b) Ex situ IR for samples taken at different states (A–E; see text for details) in (a).

of redox peaks, of which the reduction peak shifts to a slightly positive potential at 0.15 V and has a lower integral area, but nearly equivalent to that of the oxidation peaks at 0.40 V, whereas the oxidation peak is essentially preserved. All the CV peak potentials were exactly consistent with the potential plateaus in the charge/discharge curves in Figure 2b, and were maintained almost unchanged in the subsequent cycles, which indicates a quite reversible one-step 2 e^- redox reaction of the carboxylate carbonyl groups in $Na_4C_8H_2O_6$. As demonstrated in Scheme 1, the redox reaction of $Na_4C_8H_2O_6$ at an average potential of 0.3 V proceeds smoothly between carboxylate carbonyl and enolate groups ($Na_4C_8H_2O_6$/$Na_6C_8H_2O_6$), accompanied by the insertion/extraction of Na ions into/from $Na_4C_8H_2O_6$.

Figure 2b shows the discharge/charge voltage profiles of the cells cycled between 1.8 V and 0.1 V at a rate of C/10. In accord with the CV evidence, only the first discharge curve exhibited a slope at 1.1–0.4 V, indicating SEI film formation on the electrode surface. Another pair of discharge/charge plateaus at 0.2 V/0.4 V is related to the reversible insertion/extraction reactions between Na^+ ions and $Na_4C_8H_2O_6$. The Na storage capability of the $Na_4C_8H_2O_6$ was calculated by deducting the capacity contributions from the Super P (80 mAh g^{-1}; Figure S8). $Na_4C_8H_2O_6$ was found to realize a reversible specific capacity of 186 mAh g^{-1}, which is about 99.6% of the theoretical specific capacity (187 mAh g^{-1}). The reversible specific capacity of the $Na_4C_8H_2O_6$ electrode keeps quite stable, from 207 mAh g^{-1} at the first cycle to 184 mAh g^{-1} after 100 cycles, giving a high capacity retention of 89%. Simultaneously, the Coulombic efficiency increased from 65% to 99% (Figure 2c). The Super P can also retain a stable capacity during cycling (Figure S8b). Figure 2d shows the rate cycling behavior of the $Na_4C_8H_2O_6$ electrode in the lower potential range at various rates. The $Na_4C_8H_2O_6$ electrode displays a reversible capacity of 213, 207, 187, 175, 149, and 117 mAh g^{-1} at C/20, C/10, C/5, 1 C, 2 C and 5 C rates, respectively. Particularly, at 5 C (935 mA g^{-1}), the electrode still delivers a reversible capacity of 117 mA h g^{-1}, exhibiting excellent rate capability.

To grasp insight into the structural evolution of Na_4DHTPA, we performed spectroscopic analysis of the electrode upon cycling within the full potential window of 0.1–2.8 V. Well-defined plateaus can be observed at 2.3 V and 0.3 V (Figure 3a). Ex situ IR spectra were collected for the pristine, fully charged, and fully discharged samples recovered from the dismantled cells (Figure 3b). The infrared spectra for the electrodes at an initial potential (2.0 V; A), discharged (1.6 V; C), and charged (1.8 V; E) are more consistent with that of the as-made Na_4DHTPA (Figure S1). The strong vibrations centered at 1556 and 1223 cm^{-1} were assigned to C=O stretching mode of carboxylate groups and the =C–O stretching mode of the enolate groups, respectively. The peak at a low frequency of 544 cm^{-1} is ascribed to the COO–Na out-of-plane bending vibration. At fully charged 2.8 V (B), the enolate groups signal disappears and a new peak at 1658 cm^{-1} shows the production of a quinonoid carbonyl group. At fully discharged 0.1 V (D), the vibration of carboxylate at 544 cm^{-1} disappears, while the enolate vibration remains. The changes of representative infrared data clearly reveal redox reactions of an enolate/quinonoid carbonyl couple at a high potential region of 1.6–2.8 V, and a carboxylate/enolate couple at a low potential interval of 0.1–1.8 V. In addition, the ex situ IR results reflect the structural stability of the Na_4DHTPA. Indeed, density functional theory (DFT) calculations also show redox reactions of an enolate/quinonoid carbonyl couple with an average potential of 2.27 V and a carboxylate/enolate couple with an average potential of 0.36 V (for computational details, see Tables S2–S5). This further supports the experimental investigation.

The outstanding capacity and cyclability at the well-defined potential window of Na_4DHTPA allows us to assemble coin-type symmetrical full cells. Figure 4 shows the typical full-cell performance. As anticipated, these cells exhibit open-circuit voltages near zero, as the initial active materials of both electrodes are the same. However, the first charging to 2.6 V and the subsequent discharging to 0.2 V give capacities of 223 and 198 mAh g^{-1}, respectively, on the basis of the $Na_4C_8H_2O_6$ mass in the negative electrode. The galvanostatic charge and discharge curves display similar sloping shapes (Figure 4a). After 100 cycles, 76% of the cell capacities were found to be accessible at a rate of 0.1 C. The

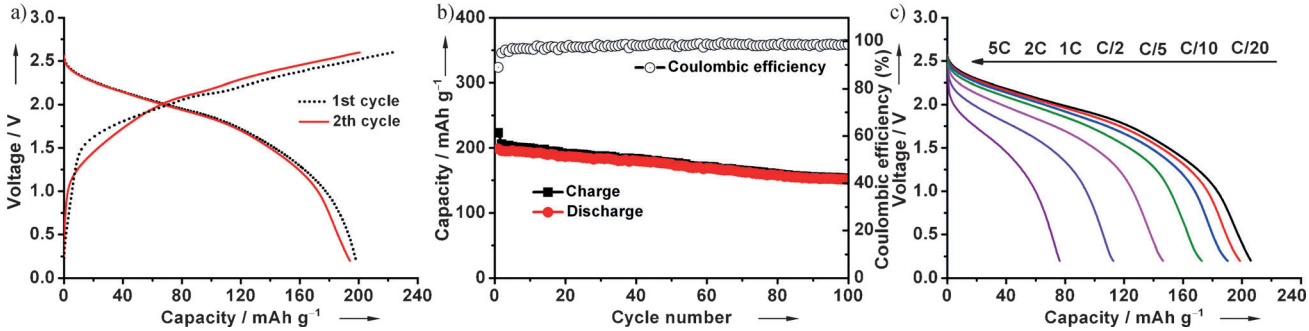

Figure 4. a) Galvanostatic charge/discharge voltage profiles of the full cells assembled with Na_4DHTPA under a current density of 19 mA g^{-1}. b) Cycling and Coulombic efficiency under a current density of 19 mA g^{-1}. c) Rate capability at various rates from C/20 to 5 C. The loading amount of the positive and negative electrode materials is about 1.8 and 1.0 mg cm^{-2}, respectively. The specific capacity is calculated based on the $Na_4C_8H_2O_6$ mass of the negative electrode with capacity contributions from the Super P.

Coulombic efficiency after initial cycles remains stable at around 99% (Figure 4b). We also evaluated the rate capability of the cells by discharging the same cell at different C rates. There is a negligible difference in discharge behavior between 0.05 and 0.2 C. Further increases beyond 0.2 C led to observable polarization, and hence lowered working voltage and reduced capacity (Figure 4c). The Na^+ shuttlecock mechanism of the full cells is also confirmed by conducting quantitative inductively coupled plasma (ICP) analysis of the Na^+ contents in the pristine, full charged and discharged states of the electrodes (Table S6). Notably, the average discharge voltage of the full cells is about 1.8 V, which approximately corresponds to the potential gap between the positive electrode (ca. 2.3 V vs. Na^+/Na) and the negative electrode (ca. 0.3 V vs. Na^+/Na). The practical energy density of the full cells are estimated to be about 65 Wh kg^{-1} by roughly assuming a one-third reduction factor related to the weight of the whole battery components. In this regard, Na_4DHTPA is promising for the construction of sustainable all-organic rechargeable sodium batteries.

In conclusion, we prepared an organic tetrasodium salt $Na_4C_8H_2O_6$ by a green and facile method, and tested its feasibility as both a positive and a negative electrode material for rechargeable SIBs. This novel material can be reversibly cycled at both potential windows of 1.6–2.8 V and 0.1–1.8 V, delivering equivalent, stable capacities larger than 180 mAh g^{-1}, and Coulombic efficiency near 100%. The reversible uptake/removal of two Na^+ ions in $Na_4C_8H_2O_6$ is separately associated with the enolate groups at 1.6–2.8 V and carboxylate groups at 0.1–1.8 V. Furthermore, starting from Na_4DHTPA as the initial active material for both the positive and negative electrodes we constructed a symmetrical all-organic rocking-chair cell with an average operation voltage of 1.8 V, a specific energy of about 65 Wh kg^{-1}, and stable cycling for over 100 cycles. The results shed light on designing organic Na-reservoir compounds as the electrode materials of rechargeable sodium-ion batteries.

Received: January 2, 2014
Published online: February 20, 2014

Keywords: batteries · electrochemistry · electrode materials · rocking-chair cell · sodium

[1] S. W. Kim, D. H. Seo, X. H. Ma, G. Ceder, K. Kang, *Adv. Energy Mater.* **2012**, *2*, 710–721.
[2] H. L. Pan, Y. S. Hu, L. Q. Chen, *Energy Environ. Sci.* **2013**, *6*, 2338–2360.
[3] V. Palomares, P. Serras, I. Villaluenga, K. B. Hueso, J. Carretero-Gonzalez, T. Rojo, *Energy Environ. Sci.* **2012**, *5*, 5884–5901.
[4] C. S. Park, H. Kim, R. A. Shakoor, E. Yang, S. Y. Lim, R. Kahraman, Y. Jung, J. W. Choi, *J. Am. Chem. Soc.* **2013**, *135*, 2787–2792.
[5] Z. L. Jian, W. Z. Han, X. Lu, H. X. Yang, Y. S. Hu, J. Zhou, Z. B. Zhou, J. Q. Li, W. Chen, D. F. Chen, L. Q. Chen, *Adv. Energy Mater.* **2013**, *3*, 156–160.
[6] S. P. Ong, V. L. Chevrier, G. Hautier, A. Jain, C. Moore, S. Kim, X. H. Ma, G. Ceder, *Energy Environ. Sci.* **2011**, *4*, 3680–3688.
[7] N. Yabuuchi, M. Kajiyama, J. Iwatate, H. Nishikawa, S. Hitomi, R. Okuyama, R. Usui, Y. Yamada, S. Komaba, *Nat. Mater.* **2012**, *11*, 512–517.
[8] Y. L. Cao, L. F. Xiao, W. Wang, D. W. Choi, Z. M. Nie, J. G. Yu, L. V. Saraf, Z. G. Yang, J. Liu, *Adv. Mater.* **2011**, *23*, 3155–3160.
[9] Y. S. Wang, X. Q. Yu, S. Y. Xu, J. M. Bai, R. J. Xiao, Y. S. Hu, H. Li, X. Q. Yang, L. Q. Chen, X. J. Huang, *Nat. Commun.* **2013**, *4*, 2365.
[10] Z. P. Song, H. S. Zhou, *Energy Environ. Sci.* **2013**, *6*, 2280–2301.
[11] Y. L. Liang, Z. L. Tao, J. Chen, *Adv. Energy Mater.* **2012**, *2*, 742–769.
[12] H. Nishide, K. Oyaizu, *Science* **2008**, *319*, 737–738.
[13] H. Y. Chen, M. Armand, G. Demailly, F. Dolhem, P. Poizot, J. M. Tarascon, *ChemSusChem* **2008**, *1*, 348–355.
[14] W. Choi, D. Harada, K. Oyaizu, H. Nishide, *J. Am. Chem. Soc.* **2011**, *133*, 19839–19843.
[15] Y. Morita, S. Nishida, T. Murata, M. Moriguchi, A. Ueda, M. Satoh, K. Arifuku, K. Sato, T. Takui, *Nat. Mater.* **2011**, *10*, 947–951.
[16] T. Nokami, T. Matsuo, Y. Inatomi, N. Hojo, T. Tsukagoshi, H. Yoshizawa, A. Shimizu, H. Kuramoto, K. Komae, H. Tsuyama, J. Yoshida, *J. Am. Chem. Soc.* **2012**, *134*, 19694–19700.
[17] Y. L. Liang, P. Zhang, J. Chen, *Chem. Sci.* **2013**, *4*, 1330–1337.
[18] W. W. Huang, Z. Q. Zhu, L. J. Wang, S. W. Wang, H. Li, Z. L. Tao, J. F. Shi, L. H. Guan, J. Chen, *Angew. Chem.* **2013**, *125*, 9332–9336; *Angew. Chem. Int. Ed.* **2013**, *52*, 9162–9166.
[19] Y. L. Liang, P. Zhang, S. Q. Yang, Z. L. Tao, J. Chen, *Adv. Energy Mater.* **2013**, *3*, 600–605.

[20] Z. P. Song, H. Zhan, Y. H. Zhou, *Angew. Chem.* **2010**, *122*, 8622 – 8626; *Angew. Chem. Int. Ed.* **2010**, *49*, 8444 – 8448.
[21] Z. P. Song, T. Xu, M. L. Gordin, Y. B. Jiang, I. T. Bae, Q. F. Xiao, H. Zhan, J. Liu, D. H. Wang, *Nano Lett.* **2012**, *12*, 2205 – 2211.
[22] H. Y. Chen, M. Armand, M. Courty, M. Jiang, C. P. Grey, F. Dolhem, J. M. Tarascon, P. Poizot, *J. Am. Chem. Soc.* **2009**, *131*, 8984 – 8988.
[23] K. Sakaushi, G. Nickerl, F. M. Wisser, D. Nishio-Hamane, E. Hosono, H. S. Zhou, S. Kaskel, J. Eckert, *Angew. Chem.* **2012**, *124*, 7972 – 7976; *Angew. Chem. Int. Ed.* **2012**, *51*, 7850 – 7854.
[24] M. Armand, S. Grugeon, H. Vezin, S. Laruelle, P. Ribiere, P. Poizot, J. M. Tarascon, *Nat. Mater.* **2009**, *8*, 120 – 125.
[25] L. Zhao, J. M. Zhao, Y. S. Hu, H. Li, Z. B. Zhou, M. Armand, L. Q. Chen, *Adv. Energy Mater.* **2012**, *2*, 962 – 965.
[26] Y. Park, D. S. Shin, S. H. Woo, N. S. Choi, K. H. Shin, S. M. Oh, K. T. Lee, S. Y. Hong, *Adv. Mater.* **2012**, *24*, 3562 – 3567.
[27] R. Zhao, L. Zhu, Y. Cao, X. Ai, H. X. Yang, *Electrochem. Commun.* **2012**, *21*, 36 – 38.
[28] K. Sakaushi, E. Hosono, G. Nickerl, T. Gemming, H. Zhou, S. Kaskel, J. Eckert, *Nat. Commun.* **2013**, *4*, 1485.
[29] H. G. Wang, S. Yuan, D. L. Ma, X. L. Huang, F. L. Meng, X. B. Zhang, *Adv. Energy Mater.* **2013**, DOI: 10.1002/aenm.201301651.
[30] K. Chihara, N. Chujo, A. Kitajou, S. Okada, *Electrochim. Acta* **2013**, *110*, 240 – 246.
[31] M. Yao, H. Senoh, H. Sano, K. Kuratani, T. Kiyobayashi, H. Sakaebe, Meeting Abstracts **2012**, MA2012-02, 1861.
[32] A. Abouimrane, W. Weng, H. Eltayeb, Y. J. Cui, J. Niklas, O. Poluektov, K. Amine, *Energy Environ. Sci.* **2012**, *5*, 9632 – 9638.
[33] W. W. Deng, X. M. Liang, X. Y. Wu, J. F. Qian, Y. L. Cao, X. P. Ai, J. W. Feng, H. X. Yang, *Sci. Rep.* **2013**, *50*, 2671.
[34] S. Komaba, W. Murata, T. Ishikawa, N. Yabuuchi, T. Ozeki, T. Nakayama, A. Ogata, K. Gotoh, K. Fujiwara, *Adv. Funct. Mater.* **2011**, *21*, 3859 – 3867.
[35] L. M. Zhu, Y. F. Shen, M. Y. Sun, J. F. Qian, Y. L. Cao, X. P. Ai, H. X. Yang, *Chem. Commun.* **2013**, *49*, 11370 – 11372.
[36] S. W. Wang, L. J. Wang, K. Zhang, Z. Q. Zhu, Z. L. Tao, J. Chen, *Nano Lett.* **2013**, *13*, 4404 – 4409.